CHEMISTRY

Framework nucleic acid strategy enables closer microbial contact for programming short-range interaction

Na Chen[1]†, Jing Xi[1]†, Na Du[1]†, Ruichen Shen[2], Rui Zhao[1], Wei He[1], Tianhuang Peng[2], Yanbing Yang[1], Yun Zhang[3]*, Lilei Yu[1]*, Weihong Tan[2]*, Quan Yuan[1,2]*

Programming precise and specific microbial intraspecies or interspecies interaction would be powerful for microbial metabolic regulation, signal pathway mechanism understanding, and therapeutic application. However, it is still of great challenge to develop a simple and universal method to artificially encode the microbial interactions without interfering with the intrinsic cell metabolism. Here, we proposed an extensible and flexible framework nucleic acid strategy for encoding the specific and precise microbial interactions upon self-assembly. With this spatial manipulation tool, we propose the microbial spatial heterogeneity and short-range interaction mechanism that the microbial assembly facilitates the gene expressions of the surface sensors including flagella and pili in *Pseudomonas aeruginosa*, leading to a more sensitive response to quorum sensing. The microbial interaction programming strategy proposed in this work is expected to provide a powerful and designable nanoplatform for better understanding of distance-dependent bacterial communication networks.

INTRODUCTION

In nature, organisms across all domains of life do not exist in isolation but form complex ecological interaction webs through dense cell interaction networks (*1*, *2*). The cell-cell interactions are indispensable for signaling and play crucial roles in life evolution and the progression of disease (*3*). Microorganisms, generally with simple cellular structures, are present in nearly every niche on earth ranging from the deep ocean, soil, air, to the human gastrointestinal tract, and are recognized as one of the earliest life forms (*4*). Microbe intercellular interactions mediated by the endogenous cell adhesion molecules scale up to determine the dynamic and functions of ecosystems and perform crucial roles in driving major global elemental cycles and evolution of ecological environment and life (*5*–*9*). Actually, microbes and humans have coexisted and interacted since the dawn of civilization (*10*). The intraspecies and interspecies interactions among microorganisms not only can maintain human health through resisting the colonization and invasion of foreign microorganisms but also can induce the progression of diseases through affecting the production of immune factors and signaling molecules to activate or inhibit key signaling pathways of host cells (*11*–*13*). The ability to program precise and specific microbial intraspecies or interspecies interactions would allow us to have a deeper understanding of the functions and behaviors of microorganisms, thus offering insights into the relationship between the microbial interaction and disease mechanism and opening vast opportunities for microbial metabolic regulation.

Native adhesion molecules such as adhesins and cadherins usually mediate the microbial interactions. With the boosting development of synthetic biology technology, researchers have artificially directed the cell interactions by overexpressing these endogenous adhesion molecules through gene editing (*14*–*17*). However, the endogenous adhesion molecules can be expressed by different cells and usually play dual roles as downstream signaling molecules, interfering with the microbial metabolic processes (*5*). The non-specificity and cross-reactivity character of the native adhesion molecules largely limit their use for programming specific and precise cell interactions (*5*, *6*). In addition to the biotechnological methods, chemical approaches, including receptor/ligand-specific binding strategies, have also been proposed (*18*–*22*). However, these methods for encoding cell interactions usually require chemical or gene editing treatment, which inevitably interferes with the intrinsic cell metabolism and sets limitations on the exploration of microbial interaction and the understanding of microbe-related disease mechanism (*23*, *24*).

Nucleic acid, encoding the genetic information of all life forms, owns the intrinsic advantages of outstanding biocompatibility, programmability, and flexibility, and has attracted numerous attention for nongenetically manipulating cell-cell interactions and functions at the nanoscale (*25*–*29*). Here, we proposed an extensible and flexible framework nucleic acid (FNA) strategy for encoding specific and precise programmable microbial interactions upon self-assembly without additional cell chemical or gene editing processing. As demonstrated in Fig. 1, DNA nanojunctions were formed through DNA hybridization between the complementary base pairing of FNAs. By simply regulating the nucleic acid sequences and sizes, the recognition domain and close-contact zone between various microorganisms can be flexibly and specifically manipulated. As a proof of concept, microbial intraspecies of *Pseudomonas aeruginosa* (*P. aeruginosa*)–*P. aeruginosa* manipulated with the FNA tools was selected as the research model. The results demonstrate that the spatial assembly of *P. aeruginosa* enhances the secretion of virulence factor, exhibiting distance-dependent heterogeneity features in microbial metabolism. According to the previous reports and the transcriptomics results in

[1]Renmin Hospital of Wuhan University, College of Chemistry and Molecular Sciences, Institute of Molecular Medicine, School of Microelectronics, Wuhan University, Wuhan 430072, P. R. China. [2]Molecular Science and Biomedicine Laboratory (MBL), State Key Laboratory of Chemo/Biosensing and Chemometrics, College of Chemistry and Chemical Engineering, Hunan University, Changsha 410082, P. R. China. [3]State Key Laboratory of Structural Chemistry, Fujian Institute of Research on the Structure of Matter, Chinese Academy of Sciences, Fuzhou 350002, China.
*Corresponding author. Email: yuanquan@whu.edu.cn (Q.Y.); tan@hnu.edu.cn (W.T.); lileiyu@whu.edu.cn (L.Y.); zhangy@fjirsm.ac.cn (Y.Z.)
†These authors contributed equally to this work.

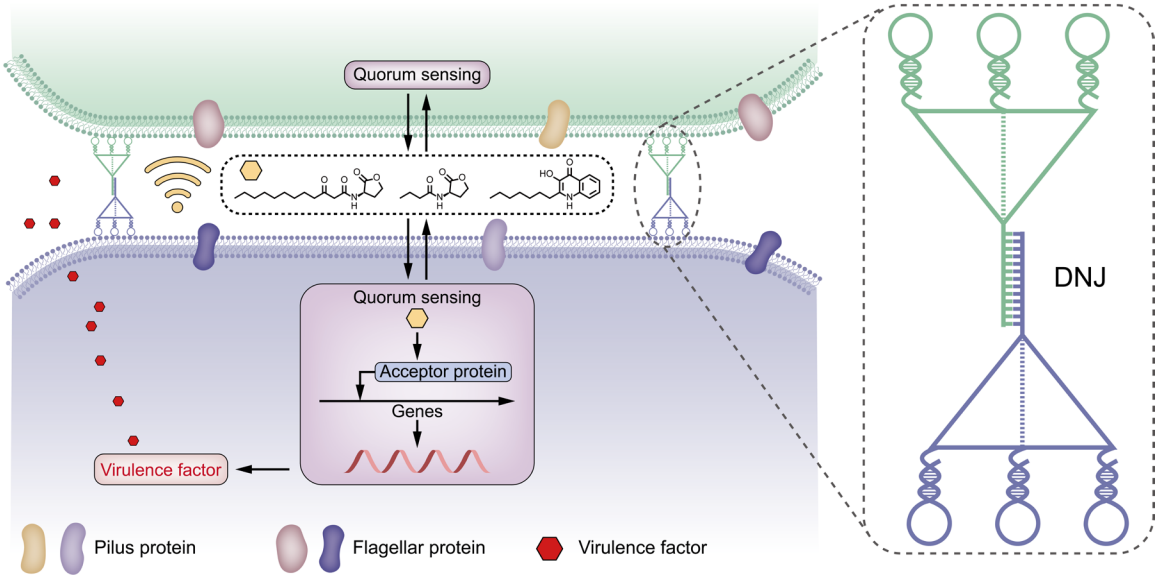

Fig. 1. Schematic illustration of the proposed FNA strategy for the specific and precise microbial interaction encoding upon self-assembly. The constructed FNAs consist of four modules including aptamer recognition module, tetrahedron distance regulation module, lock-and-key linking module, and fluorescence reporting module, offering platform for microbial interaction mechanism exploration. DNJ, DNA nanojunctions.

this work, we propose the microbial heterogeneity mechanism that the short-range interaction mediated with the constructed FNAs induces the overexpression of surface sensor including flagella and pili in *P. aeruginosa*, thus leading to more sensitive responses to quorum sensing (QS) and higher levels of virulence factor. In addition, we demonstrate that the FNA platform shows universality in programming interactions among microbes and can both encode the specific intraspecies and interspecies interactions with the rationally designed flexible nucleic acid sequences. Overall, the proposed microbial interaction encoding toolbox may pave ways for programming high-level multicellular biological systems and shed light on the distance-dependent heterogeneity of microbial metabolism to discovery potential communication rules.

RESULTS

Constructing and characterizing of FNAs

The spatial structure of microbial communities is recognized to affect ecological stability, functional activities, and the responses to environmental perturbations (*30*). Microorganism usually has its communication range that is defined as the distance from the boundary of signal producer over which the signal response reduces one order of magnitude (*31*). Regulating and programming the spatial distance between microorganisms would facilitate the exploration of the microbial interaction mechanism and the communication behaviors (*32*). *P. aeruginosa*, a predominant Gram-negative bacterium within the hospital environment, is the pathogen responsible for severe opportunistic pulmonary infections (*33*–*35*). Here, we adopted the *P. aeruginosa* as the research model and the corresponding FNAs were constructed for manipulating the *P. aeruginosa*–*P. aeruginosa* interaction.

As shown in Fig. 2A, the FNA pairs obtained through self-assembly both include four functional modules: recognition module, distance regulation module, "lock-and-key" linking module, and reporting module. To be specific, recognition module is the corresponding nucleic acid aptamers, which are single-stranded DNA or RNA sequences generated through a repetitive process of in vitro selection with the ability to specifically bind the target molecules. In our design, multivalent pattern recognition strategy was adopted to further increase the binding affinity and targeting ability of aptamer (*29*). In addition, the distance regulation module is the DNA tetrahedrons with a defined dimension, enabling the precise control over the microbial interaction spacing (*26*). A single dangling DNA strand at the top vertex of the tetrahedral structure enables the specific linking through the complementary base pairing principle, acting as part of the lock-and-key linking module. Simultaneously, fluorescence resonance energy transfer signal between cyanine-3 (Cy3)–labeled framework and Cy5-labeled framework enables to report the real-time and dynamic information reporting for the linking process. Overall, taking the unique advantages of flexibility and programmability of nucleic acid molecules, we propose an extendable technique on the basis of DNA self-assembly.

Construction of FNAs was first characterized by gradually slower gel migration of the DNA mixture with a step-by-step addition of reactant DNA strands (Fig. 2B and table S1). The results of atomic force microscopy (Fig. 2C) and dynamic light scattering (Fig. 2D) further confirmed the successful construction of FNAs. In addition, by modifying optical labels of Cy3 and Cy5 respectively in the dangling DNA strand, the labeled FNA pairs tend to have an optical signal change when the chain links and the energy transfer occurs as illustrated in Fig. 2E, thus providing a real-time and dynamic view for the linking process (fig. S1). As expected, it can be clearly observed that a new emission peak at 670 nm appeared with the excitation at 535 nm, while the emission intensity at 565 nm decreased in Fig. 2F.

FNAs induced microbial assembly in *P. aeruginosa*

The confocal images in Fig. 2G show representative *P. aeruginosa* aggregates in the DNA framework pair treated group, while the

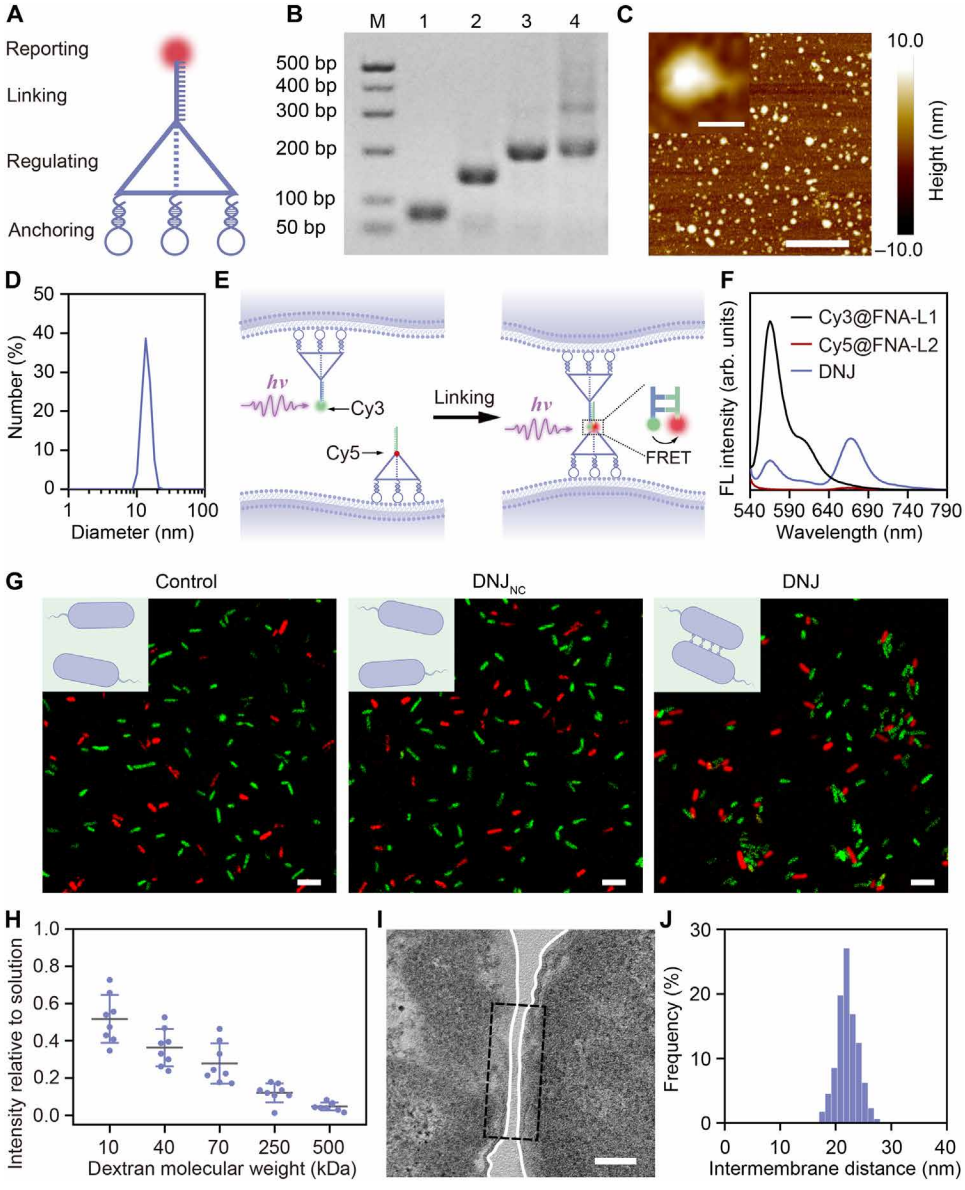

Fig. 2. Construction of the multifunctional FNAs and the specific assembly of *P. aeruginosa*. (**A**) Schematic of the multifunctional FNAs consisted of anchoring section, regulation section, linking section, and reporting section for the precise manipulation of the close-contact zone for microbial assembly. (**B**) Polyacrylamide gel electrophoresis analysis of the formation of the FNAs. From lane 1 to lane 4 of each panel, different reactant DNA strands were gradually added. Lane M was loaded with a 50–base pair (bp) DNA marker. (**C**) Atomic force microscopy images of the constructed FNAs. Scale bars, 200 nm (original images) and 20 nm (enlarged view). (**D**) Dynamic light scattering measurements of the size distribution of the constructed FNAs. (**E**) Schematic of the assembly reporting process based on fluorescence resonance energy transfer (FRET). (**F**) Fluorescence (FL) intensity of the FNA pairs. (**G**) Confocal laser scanning microscope (CLSM) images of *P. aeruginosa* after incubation with 200 nM FAM-labeled FNA and Cy5-labeled FNAs for 20 min. Scale bars, 5 μm. (**H**) Relative fluorescence intensity of dextrans with different molecular weights at the cellular contact zone. Data are represented as means ± SD (n > 10 from different cellular contacts). (**I**) Transmission electron microscopy (TEM) images of FNA pairs mediated contact between *P. aeruginosa*. Scale bar, 100 nm. (**J**) The intermembrane distances are measured on the basis of the TEM images and grouped in 2-nm intervals. All the incubation concentrations of the FNAs in these experiments were fixed at 200 nM.

P. aeruginosa in the control groups has a random distribution, suggesting a spatial manipulation for microbial interaction programming. In addition, the specificity and targeting performances were further explored in *P. aeruginosa*–*Staphylococcus aureus* coculture with different morphologies. The *P. aeruginosa* incubated with Cy3-labeled FNAs containing aptamer section displays an obvious fluorescent shift, whereas no obvious fluorescence change is observed for *P. aeruginosa* incubated with Cy3-labeled FNAs without aptamer section, suggesting that the aptamer exhibits much stronger binding affinity and specificity toward *P. aeruginosa* (fig. S2). Figure S3 shows that the rod-shaped *P. aeruginosa* was aggregated, while the spherical *S. aureus* was randomly distributed after the treatment of the corresponding FNA pairs. The above results validate the excellent specificity and targeting performance of the designed FNAs (figs. S4 to S7).

To further explore the microbial interaction manipulation ability of the constructed FNA pairs, a size-dependent diffusion strategy using fluorescein isothiocyanate–labeled dextrans of different molecular weight was adopted. As shown in Fig. 2H, the fluorescein isothiocyanate (FITC) fluorescence decreased with the increase of dextran size, suggesting a hindered diffusion into the cellular surface with higher dextran molecular weight. According to the size of the dextran in figs. S8 and S9, it is suggested that the intermembrane gap can be estimated to be around 23 nm, which is consistent with the FNA size in theory (fig. S10). In addition, the transmission electron microscopy (TEM) image in Fig. 2I shows clear spatial gaps at cellular interface mediated with the FNA pairs. The intermembrane gap was calculated to be around 22 nm as shown in Fig. 2J, agreeing well with the expected value. It is worth mentioning that the tetrahedron structure can be flexibly and rationally designed by adjusting the DNA sequences to regulate the size precisely (figs. S11 to S13 and table S2) (*26*). Collectively, the above results demonstrate that the constructed DNA frameworks are capable of the specific and precise programming for microbial interactions in real.

FNAs induced microbial heterogeneity

Microorganisms are known to communicate with neighboring ones with a distance of up to several micrometers by secreting and sensing signaling molecules (*36*, *37*). Signal molecules are generally thought to broadly diffuse in space, offering information about the overall composition of the community (*38*, *39*). The spatial proximity of community members directly determines the diffusion distance of the signaling molecules, playing critical roles in regulating their activities in social networks and shaping the evolution of ecological networks (*30*, *31*, *40*, *41*). It has been widely recognized that *P. aeruginosa* can regulate the multi-behaviors such as virulence factor generation and horizontal resistance gene transfer through communicating and dealing with signaling molecules (*35*, *42*, *43*). As a proof of concept, the intraspecies interaction of *P. aeruginosa* was selected as the research model. With the constructed corresponding FNA pairs, the interactions and metabolic behaviors have been explored.

Figure 3A shows that the OD_{600} (optical density at 600 nm) values of *P. aeruginosa* treated with the constructed FNA pairs are higher across time compared with the ones in bare *P. aeruginosa*. In addition, it can also be observed that the OD_{600} values both tend to be stable and fix at around 2.8 cultured at the later stage of 48 hours. The above results indicate that the manipulation of the spatial distance between *P. aeruginosa* facilitates the microbial growth at the early stage and stay stable later. The regulated microbial behavior can be owing to the increased exchange of nutriments and signal molecules by shortening the microbial distance, and the final OD_{600} values both tend to be stable limited by the nutriment (*37*). It has been previously pointed out that the *P. aeruginosa* is able to adapt to the adverse environment in hosts by secreting a variety of virulence factors such as rhamnolipid and exotoxin A, which play key roles in host infection and immune response (*44*). Subsequently, the virulence factor synthesis processes of *P. aeruginosa* were further explored with the constructed FNA pairs. As shown in Fig. 3 (B and C), it can be observed that the virulence factors including rhamnolipid and exotoxin A both have higher concentrations in *P. aeruginosa* treated by the constructed FNA pairs compared with the ones in bare *P. aeruginosa*. The results indicate that the short-range interaction manipulated using the FNA toolbox enables facilitating the production of virulence factors, which undoubtedly leads to increased pathogenicity (fig. S14). Overall, the above results validate a spatial metabolism heterogeneity in *P. aeruginosa* and demonstrate that both the population and metabolic behaviors differ at spatial scale.

Considering that virulence factors affect host's health, we then adopt A549 human pulmonary epithelial cells as the research model to further investigate the influence of microbial spatial heterogeneity on host (*43*). By incubating A549 cells with the microbial supernatant containing the secreted virulence factors, we found that the A549 cells incubated with the supernatant of assembled *P. aeruginosa* demonstrate higher concentrations of pro-inflammatory factors including interleukin-6 (IL-6), IL-8, and tumor necrosis factor–α (TNF-α) compared with the ones in A549 incubated with the supernatant of the unassembled *P. aeruginosa* (Fig. 3, D to F). The higher levels of pro-inflammatory factors suggest that the inflammatory signaling pathways such as nuclear factor κB pathway are activated and that the inflammatory responses are triggered (*44*–*47*). The results demonstrate that the short-range interactions in *P. aeruginosa* manipulated with the constructed FNA pairs affect the inflammatory response of the A549 host metabolism by influencing the secretion

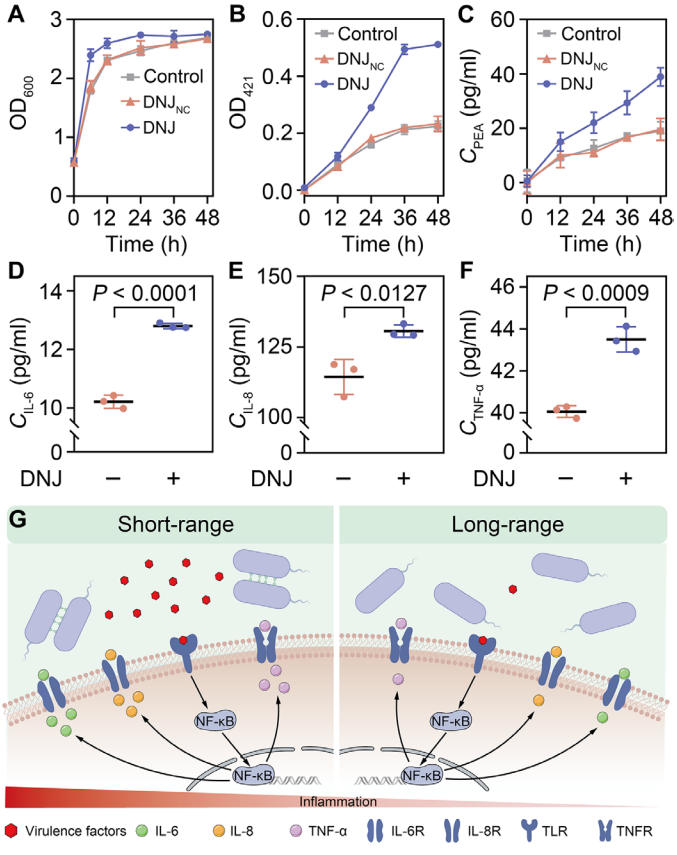

Fig. 3. The short-range interactions mediated by the constructed FNA pairs enhance the pathogenicity of *P. aeruginosa*. (**A**) OD_{600} (optical density at 600 nm) values of *P. aeruginosa* across time. Data presented as means ± SD, $n = 3$. (**B** and **C**) Concentrations of virulence factors including (B) rhamnolipid and (C) exotoxin A in *P. aeruginosa* solution. Data presented as means ± SD, $n = 3$. h, hours. (**D** to **F**) Concentrations of inflammatory factors including (D) interleukin-6 (IL-6), (E) IL-8, and (F) tumor necrosis factor–α (TNF-α) in A549 cells. Data presented as means ± SD, $n = 3$. (**G**) Schematic illustration showing the influence of short-range interactions on the inflammation in A549 cells. NF-κB, nuclear factor κB; TLR, Toll-like receptor; TNFR, tumor necrosis factor receptor.

of virulence factors (Fig. 3G). According to the above results, the proposed FNA strategy is expected to provide reliable platforms and tools for the analysis of microbial spatial heterogeneity and microbial-host interactions. Considering that the communication networks within the microbial species triggered markedly different inflammation level, suggesting that the immune responses can be induced with the FNAs, which might offer thoughts for the biomedical applications such as vaccine development (*48*).

Molecular mechanism of short-range interactions in enhancing pathogenicity of *P. aeruginosa*

To have an in-depth understanding of the short-range interaction mechanism of *P. aeruginosa* mediated by the constructed FNA pairs, transcriptomic analysis was further performed. Differentially expressed genes were evaluated according to the $\log_2$ fold change ($\log_2$ FC) values, which were calculated with the formula of $\{\log_2 [(\text{FPKM})_{(\text{Experimental})}] - \log_2 [(\text{FPKM})_{(\text{Control})}]\}$. As shown in Fig. 4A, of 5476 transcripts detected in *P. aeruginosa*, 860 were associated with the short-range interaction ($P < 0.05$ and FC > |1.5|), suggesting that the short-range interaction mediated by the constructed FNA pairs affects the gene expressions of *P. aeruginosa*. Overrepresented (white to red) and underrepresented (white to purple) transcripts with the reference of gene expressions in unassembled culture shown as $\log_2$ FC were exhibited in Fig. 4B. It can be found that the $\log_2$ FC values of pilus and flagellum are both >0 on the whole, suggesting that the genes encoding pilus and flagellum were actively expressed by manipulating the spatial distance with the constructed FNA pairs. Pilus and flagellum have been reported to promote the adhesion ability of *P. aeruginosa*. Hence, it was rationalized that the spatial assembly driving force of *P. aeruginosa* might be derived from two aspects: (i) the hydrogen bond interaction of the constructed FNAs through complementary base pairing and (ii) the overexpressed adhesion molecules including the pilus and flagellum.

Apart from the adhesion ability, pilus and flagellum can also act as surface sensors for hyperresponsive to QS signaling molecules according to the previous studies (*49*). Figure 4C shows that the $\log_2$ FC of genes associated with QS system is also >0 on the whole, suggesting that the QS system was activated through spatial manipulation with the constructed FNAs. To some extent, the activated QS system can be rationalized to the more sensitive response to QS signaling molecules through the overexpressed surface sensors (*49*). In addition, the QS signaling molecules including *N*-butyryl-L-homoserine

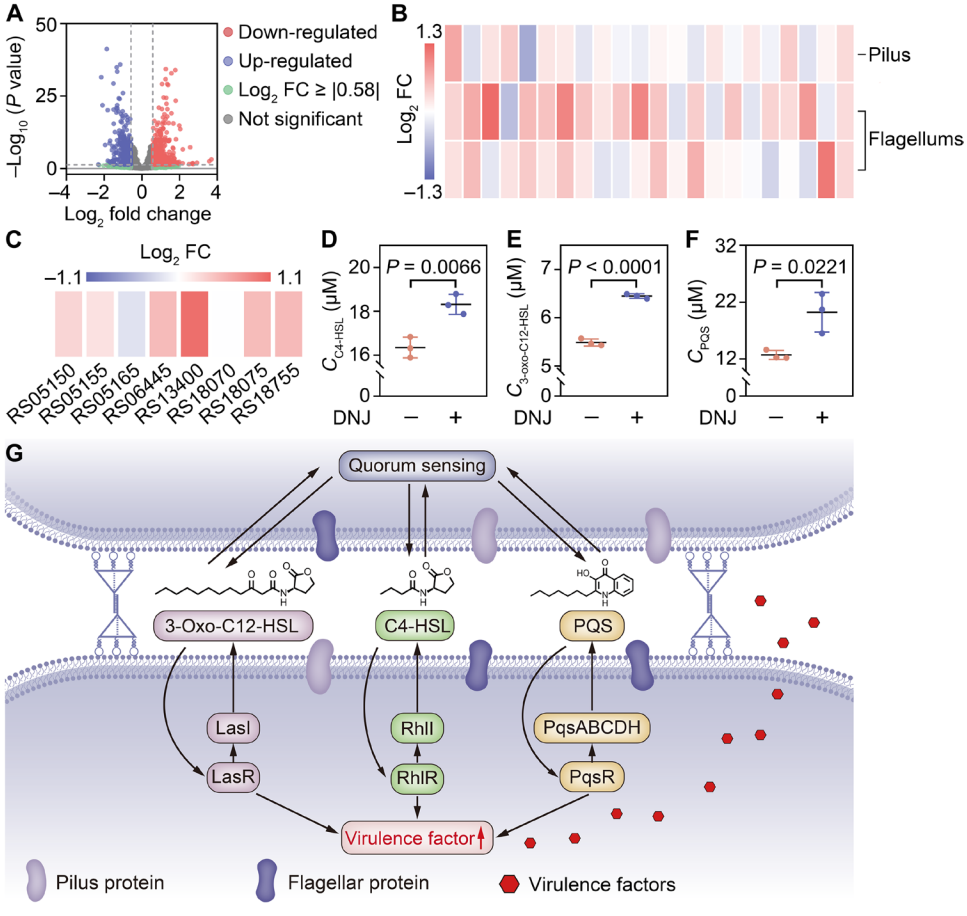

Fig. 4. Spatial metabolic heterogeneity mechanism of the intraspecies interaction in *P. aeruginosa*. (**A**) A Volcano plot of differentially expressed genes in *P. aeruginosa*. The threshold of $\log_2$ FC is |0.58| (i.e., FC ≥ |1.5|) and that of *P* value is <0.05. There were 860 differentially expressed microbial transcripts that met these criteria. (**B**) Genes expression heatmaps of pilus and flagellum. (**C**) Gene expression heatmaps associated with the QS system. (**D** to **F**) Concentrations of QS signal molecules including (D) C4-HSL, (E) 3-oxo-C12-HSL, and (F) PQS in *P. aeruginosa*. Data presented as means ± SD, $n = 3$. (**G**) Schematic illustration of spatial metabolic heterogeneity mechanism of *P. aeruginosa*.

lactone (C4-HSL), *N*-(3-Oxododecanoyl)-L-homoserine lactone (3-oxo-C12-HSL), and 2-heptyl-3-hydroxy-4(1H)-quinolinone (PQS) are all demonstrated to have higher concentrations after the treatment of the constructed FNA pairs in assembled *P. aeruginosa* compared with the ones in unassembled *P. aeruginosa* (Fig. 4, D to F), further validating that the QS system is activated. Together, the increased concentrations of QS molecules can be ascribed to the positive feedback loop between the spatial manipulation tool of FNA pairs and the QS system.

In addition, by assessing the mRNA expression level, it was also found that the $\log_2$ FC values of virulence factor synthesis–associated genes in *P. aeruginosa* are >0 on the whole, suggesting an enhanced pathogenicity in *P. aeruginosa* treated with the constructed FNA pairs (fig. S15). Accordingly, on the basis of the above results, we rationalize that the short-range interactions mediated by the constructed FNA pairs enable the up-regulation of the gene expressions associated with the surface sensor of pilus and flagellum, thus enhancing the QS response sensitivity in *P. aeruginosa* and increasing the microbial pathogenicity (Fig. 4G). The proposed short-range interaction mechanism in *P. aeruginosa*, to some extent, explains why biofilms are more pathogenic than planktonic cells (*50*).

FNAs for encoding interspecies interactions

In nature, microorganisms do not live as single species but rather they coexist in a mixed one. Typically, microbial coculture coordinates specific activities by trading metabolites, exchanging signals, or integrating pathways to estimate the stability, functionality, and dynamic of communities (*51*–*54*). Subsequently, to explore the universality of the proposed FNA strategy in programming microbial interactions, the more complex interspecies interactions were further programmed and explored. *Escherichia coli* is one of the most common bacteria in the gut microbiota of humans and other animals and often induces pneumonia together with *P. aeruginosa* (*55*, *56*). Then, the interspecies interaction model of *P. aeruginosa*–*E. coli* was further adopted.

First, on the basis of the aptamer sequences of *E. coli* and *P. aeruginosa* (table S3) (*57*), the corresponding FNA pairs are rationally designed for the specific and precise programming of the interspecies interaction of *P. aeruginosa*–*E. coli* (Fig. 5A and figs. S16 to S20). The confocal images in Fig. 5B exhibit the *P. aeruginosa*–*E. coli* aggregates in the FNA-treated group, suggesting a successful spatial manipulation for *P. aeruginosa*–*E. coli*. As shown in fig. S21, it can be observed that the fluorescence intensities of the supernate in FNA-Cy3–labeled *P. aeruginosa* after different incubation time unchanged, suggesting the durability and stability of the FNA labeling over time. Figure S22A shows that the OD_{600} values are higher in *P. aeruginosa*–*E. coli* coculture treated with the designed FNAs compared with those in the bare *P. aeruginosa*–*E. coli* coculture, indicating that the spatial manipulation with the constructed FNAs facilitates the microbial growth on the whole. In addition, the proportions of *P. aeruginosa* cultured were found to be lower at 24 hours in FNA-treated groups as shown in fig. S22B. The above results indicate that the short-range interactions mediated by the constructed FNAs modulate both the metabolism behaviors and the population compositions of the microbial community.

In the same way, the mechanism of the short-range interaction between *P. aeruginosa*–*E. coli* was further explored by quantitatively measuring the virulence factors, QS signal molecules, and the associated gene expressions. As shown in Fig. 5 (C to F), it can be found that both the signal molecules and virulence factors have lower concentrations in the supernatant of *P. aeruginosa*–*E. coli* coculture after the treatment of FNAs, suggesting a decreased pathogenicity of the assembled *P. aeruginosa*–*E. coli* (fig. S23). The weak and masked QS signal molecules in assembled *P. aeruginosa*–*E. coli* can be ascribed to the distance-dependent uptake efficiency by the signal-absorbing systems in *E. coli* (*31*), and the decreased virulence factor levels are suggested to be the results of environmental adaptation for *E. coli*. The above results also demonstrate the distance-dependent metabolic heterogeneity by programming the short-range interaction between the *P. aeruginosa* and *E. coli* with the constructed FNAs. Transcriptomic results demonstrate that the gene expressions associated with QS system (Fig. 5G), pilus, flagellum, and virulence factor (figs. S24 and S25) are all down-regulated on the whole in *P. aeruginosa* upon the FNA treatment, which are quite opposite with the results in intraspecies interactions in *P. aeruginosa*. The above results indicate that the microbial short-range communication and behaviors are quite different between separate species. To some extent, this finding offers thoughts into microbial metabolism coordination by regulating the microbial communication process. In addition, inflammatory factor concentrations of IL-6, IL-8, and TNF-α in the cultured supernate of A549 cells are demonstrated to be lower when incubated with the supernate of assembled *P. aeruginosa*–*E. coli* coculture compared with the ones of unassembled system (Fig. 5, H to J), which can be ascribed to the lower concentration of virulence factors. Collectively, the above results demonstrate that our proposed FNA strategy shows universal application in both intraspecies interaction and interspecies interaction programming (Fig. 5K) and enables the discovery of distance-dependent communication rules.

DISCUSSION

In summary, we report a flexible FNA strategy for the specific encoding of microbial intraspecies or interspecies interaction by the precise manipulation of the distance between microorganisms. By rational nucleic acid sequence design, the recognition domain and close-contact zone between various microorganisms can be flexibly and specifically manipulated. Actually, with the flexible programmable advantages, other functions that have not been mentioned in this work can also be achieved. For example, by rational design, FNAs containing unpaired linker sequences can be obtained first. Only when the corresponding DNA linker is provided, the FNAs can then be paired through the hydrogen bond interaction, thus achieving the precise manipulation of the assembly process. On the basis of the constructed FNA toolbox, we propose the microbial spatial heterogeneity mechanism that the short-range interaction facilitates the gene expression of the surface sensors including flagella and pili in *P. aeruginosa*, leading to a more sensitive response to QS. The activated QS system subsequently results in a higher level of virulence factor and a stronger inflammatory impact on host cells. To some extent, the proposed short-range interaction mechanism in *P. aeruginosa* offers evidence for the increased pathogenicity of biofilms compared with that in the planktonic cells. In addition, we demonstrate that the FNA platform shows universality in programming interactions among microbes. The specific interspecies interactions of *P. aeruginosa*–*E. coli* were further successfully programmed with the rationally designed flexible nucleic acid sequences. Our proposed strategy, which leverages FNAs, excels over alternative encoding methods by offering enhanced universality, programmability, specificity, and a lack of cross-reactivity,

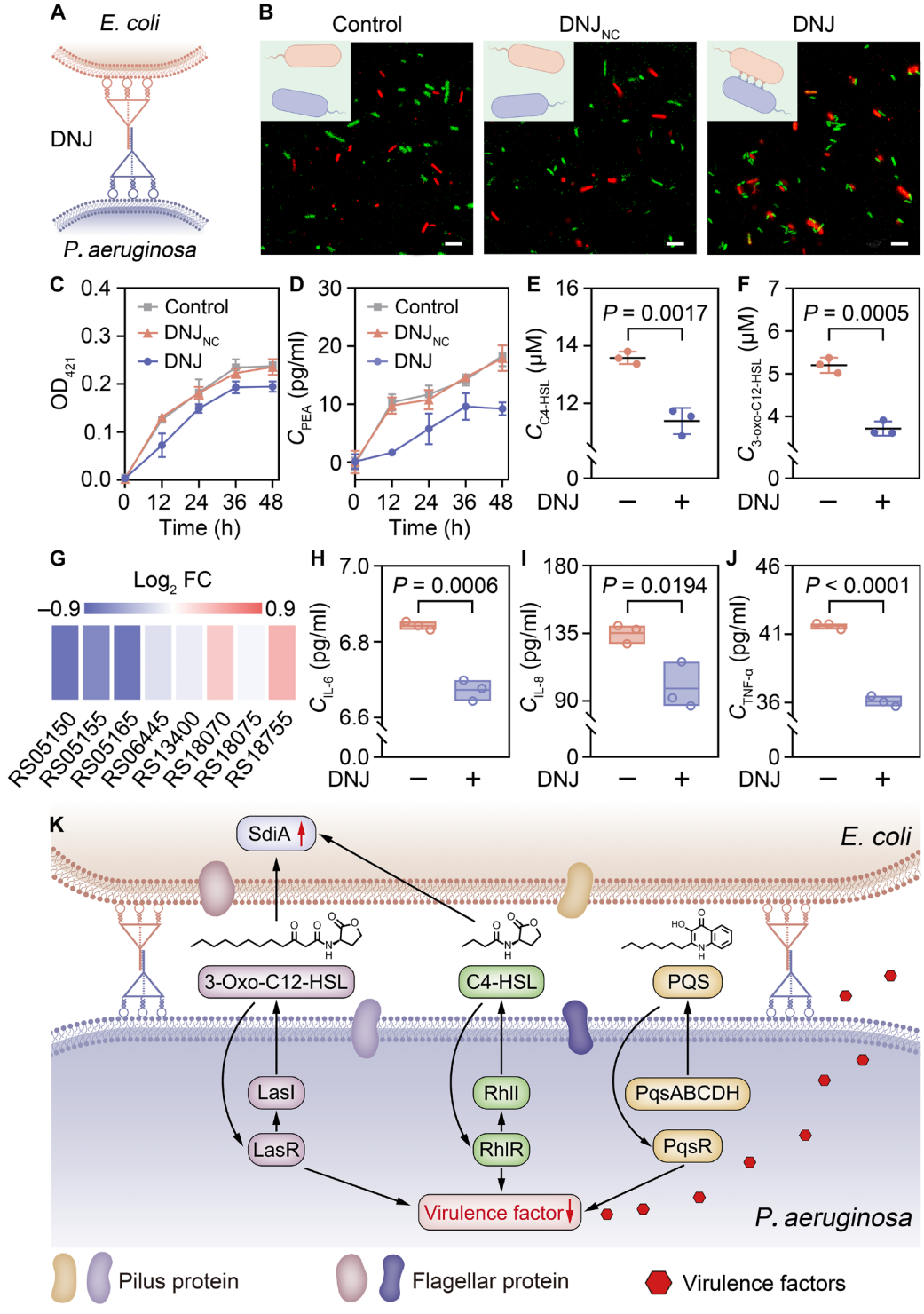

Fig. 5. Spatial metabolic heterogeneity mechanism in interspecies interactions of *P. aeruginosa*–*E. coli*. (**A**) Schematic illustration of the programmed interspecies interactions with the FNA strategy. (**B**) CLSM images of *P. aeruginosa* (green) and *E. coli* (red). Scale bars, 6 μm. (**C** and **D**) Concentration of virulence factors including (C) rhamnolipid and (D) exotoxin A in *P. aeruginosa*–*E. coli* solution. Data presented as means ± SD, $n = 3$. (**E** and **F**) Concentration of QS signal molecules including (E) C4-HSL and (F) 3-oxo-C12-HSL in *P. aeruginosa*. Data presented as means ± SD, $n = 3$. (**G**) Heatmaps of genes expressions associated with QS. (**H** to **J**) Concentration of inflammatory factors including (H) IL-6, (I) IL-8, and (J) TNF-α in A549 cells. Data presented as means ± SD, $n = 3$. (**K**) Schematic illustration of the spatial metabolic heterogeneity mechanism in *P. aeruginosa*–*E. coli*.

making it a superior choice for advanced applications. On the whole, the proposed FNA platform in this work provides robust ways for programming microbial biological systems and sheds light on the microbial spatial heterogeneity and short-range interaction mechanism exploration. Looking forward, with the development of synthetic biology, we believe that the proposed FNA platform may pave ways for flexible and controlled microbial interaction regulation and is promising in industries related to microbial metabolism such as biomanufacturing and therapeutic applications.

MATERIALS AND METHODS

Chemicals and materials

Magnesium chloride hexahydrate ($MgCl_2{\cdot}6H_2O$), nickel chloride ($NiCl_2$), agarose, ethyl acetate, and 3,5-dihydroxytoluene were purchased from Sinopharm Chemical Reagent Co. Ltd. Concentrated sulfuric acid (H_2SO_4), sodium chloride (NaCl), 2.5% glutaraldehyde, C4-HSL, 3-oxo-C12-HSL, acetonitrile, methanol, and chloroform were purchased from Aladdin Biochemical Technology Co. Ltd. PQS was purchased from Macklin Biochemical Co. Ltd. Peptone, yeast extract, agar, phosphate-buffered saline (PBS) buffer (pH 7.2 to 7.4), tris-HCl buffer (pH 8), and 50× tris-acetate-EDTA (TAE) buffer were provided by Solarbio Science & Technology Co. Ltd. SerRed Nucleic acid dyes were purchased from Servicebio Technology Co. Ltd. Trypsin-EDTA, penicillin, and streptomycin were provided by Life Technologies Corporation, USA. Ham's F-12K (Kaighn's) medium and fetal bovine serum (FBS) were purchased from Thermo Fisher Scientific Inc. The bacteria strains *P. aeruginosa* (CCTCC AB 93066), *E. coli* (CCTCC AB 2012883), and the human pulmonary epithelial cell A549 (GDC0063) were provided by China Center for Type Culture Collection (CCTCC). DNA sequence, human TNF-α enzyme-linked immunosorbent assay (ELISA) kit, human IL-8 ELISA kit, and human IL-6 ELISA kit were provided by Sangon Biotechnology Co. Ltd. Exotoxin A ELISA kit was provided by Ruixin Biotechnology Co. Ltd. The ultrapure water was obtained using a Millipore water purification system.

Characterization

Atomic force microscope (Park NX10, Korea) and nanoparticle size analyzer (Malvern Nano-ZS ZEN3600 Zetasizer, UK) were used to characterize the size of constructed FNA nanostructures. BioTek Synergy H1 microplate reader was adopted to test the absorbance of the samples. The concentration of bacteria was determined by OD_{600} using Shimadzu UV-2550 ultraviolet (UV)–visible spectrophotometer. The fluorescence performance was measured on a HORIBA QM8000 fluorescence spectrometer (HORIBA, Japan). Laser confocal images were obtained on the Olympus FluoView FV3000 confocal microscope system (Olympus, Japan). The TEM images of bacteria assemblies were obtained on a transmission electron microscope (TEM) (Hitachi, HT7700, Japan). The target efficiency of the constructed FNAs toward bacteria was obtained on the Beckman CytoFLEX S flow cytometry (Beckman, USA). The Agilent 1260 Infinity HPLC system (Agilent, USA) was used to measure the concentration of QS signal molecules including C4-HSL, 3-oxo-C12-HSL, and PQS.

Preparation of FNAs

For the synthesis of FNAs, we first adopted the Mfold software to calculate the thermal stability of DNA hybridization for each FNA (table S4). On the basis of these theoretical values, we applied specific reaction conditions for the assembly of individual FNAs. For the preparation of FNA-17, four given oligonucleotides (A-L1, B, C, and D; or A-L2, B, C, and D) were mixed together at an equal molar ratio in 500 μl of tris-HCl buffer (20 mM, pH 8.0) containing 12.5 mmol $MgCl_2$. The concentration of each oligonucleotide in the reaction solution was fixed at 2 μM. The mixed solution was then heated at 95°C for 10 min and cooled fast on ice. Subsequently, the prepared FNA-17 with a final concentration of 2 μM was obtained. For the preparation of FNA-37 for programming *P. aeruginosa* interaction, eight given oligonucleotides (A37.1-L, A37.2, B37.1, B37.2-P, C37.1, C37.2-P, D37.1, and D37.2-P) were mixed together at an equal molar ratio in 500 μl of tris-HCl buffer (20 mM, pH 8.0) containing 12.5 mmol $MgCl_2$. The concentration of each oligonucleotide in the reaction solution was fixed at 2 μM. The mixed solution was then processed according to the programmed annealing procedure (table S5). Subsequently, the prepared FNA-37 with a final concentration of 2 μM was obtained. The resultant DNA products were stored at 4°C for further use. The sequences of all these oligonucleotides are listed in table S1. All the DNA oligonucleotides were synthesized and purified with high-performance liquid chromatography (Sangon Biotech).

Agarose gel electrophoresis

To confirm the assembly of the constructed FNAs, a clear and transparent gel-like solution was prepared by adding 3.0 g of agarose and 20 μl of SerRed nucleic acid dye to 100 ml of 1× TAE buffer [40 mM tris, 20 mM acetic acid, 2 mM EDTA, and 12.5 mM $MgCl_2$ (pH 8.0)]. FNA samples (10 μl) with a concentration of 1 μM were run at 90 V for 30 min and then imaged under a UV detector.

Atomic force microscopy imaging

The FNA sample (15 μl) was mixed with $NiCl_2$ (300 μM, 5 μl) for 5 min. The mixture was then deposited on mica and dried for 10 min. After being rinsed with 80 μl of solution [20 mM tris and 50 mM $MgCl_2$ (pH 8.0)] and dried in nitrogen atmosphere, the sample was imaged using the tapping mode and analyzed with the NanoScope analysis software.

Bacterial culture

P. aeruginosa, *E. coli*, and *S. aureus* were cultured with LB medium. Each liter of LB medium contained 10 g of tryptone, 5 g of yeast extract, and 5 g of sodium chloride. The bacteria were cultured at 37°C with a rotation speed of 220 rpm. The absorbance of the bacterial culture (OD_{600}) was measured by using a Shimadzu UV-2550 UV-visible spectrophotometer to evaluate the bacterial growth density.

Cell viability tests

The colony-forming unit (CFU) was performed to determine the viability of *P. aeruginosa*. Specifically, the bare *P. aeruginosa* and *P. aeruginosa*–FNA coculture solution at different culture time (24 and 48 hours) was transferred into the LB solid medium, respectively. After 24 hours of growth at 37°C, white circular colonies can be observed. The CFU per milliliter can be determined by counting the colonies.

Anchoring specificity of the constructed FNA pairs in microbial assembly

Cultured *P. aeruginosa* and *S. aureus* with different morphologies were centrifugated and washed twice with 20 mM tris-HCl buffer

and then mixed in equal proportions with 20 mM tris-HCl buffer to reach an OD_{600} value of 0.6. Furthermore, FNA-Cy5 dye was added to the mixed bacterial solution and incubated at 37°C for 30 min. The incubated solution was then centrifugated and washed. Last, the specific target ability of FNAs to *P. aeruginosa* was assessed using an Olympus FV3000 confocal microscopy imaging system.

Confocal fluorescence microscopy imaging of bacteria assembled with FNAs

The cultured *P. aeruginosa* or *E. coli* was washed twice with 20 mM tris-HCl buffer and resuspended in the same buffer to reach an OD_{600} value of 0.6. Separate aliquots of the bacterial suspension were then mixed with 5-carboxyfluorescein (FAM) or Cy5 dyes and then washed twice with tris-HCl buffer to obtain FAM- and Cy5-labeled bacteria. Subsequently, the labeled FAM and Cy5 bacteria were incubated with the constructed FNA-1 (250 nM) and FNA-2 (250 nM) for 30 min at 37°C, respectively. Last, bacterial suspensions anchored with FNA-1 and FNA-2 were mixed in equal proportions and incubated at 37°C for 30 min to encode the bacterial assemblies. The bacteria assembled with FNAs were subsequently visualized using a confocal microscopy imaging system.

The spatial dimensions between the FNA-assembled bacteria were further characterized on the basis of the molecular diffusion principles. Specifically, FITC-labeled dextran with molecular weights of 10.0, 40.0, 70.0, 250.0, and 500.0 kDa was added to the bacterial assembly solutions. The fluorescence intensity of the bacterial assemblies was observed and recorded using a confocal microscopy imaging system.

Optical monitoring of the assembly process

The bacterial assembly process was optical monitored with the designed FNA-1–Cy3 and FNA-2–Cy5 based on Förster resonance energy transfer. To be specific, bacterial suspension was mixed with constructed FNA-1–Cy3 (250 nM) or FNA-2–Cy5 (250 nM), respectively, and then washed twice with tris-HCl buffer to remove the unanchored FNA-1–Cy3 or FNA-2–Cy5. Then, separate aliquots of the bacterial anchored with FNA-1–Cy3 and FNA-2–Cy5 were mixed to obtain the bacterial assembled solutions. Fluorescence emission was then recorded using a HORIBA QM8000 fluorescence spectrometer under 535-nm wavelength excitation for FNA-1–Cy3–labeled bacterial suspension, FNA-2–Cy5–labeled bacterial suspension, and bacterial assembled solutions.

TEM imaging

P. aeruginosa was separately decorated with FNA-1 and FNA-2 pairs and then mixed in a ratio of 1:1. The resultant assembled samples were processed with light fixation by using 2.5% glutaraldehyde and then treated with 1.0% osmium tetroxide and 0.5% uranyl acetate. Subsequently, 25, 50, 75, and 100% ethanol solution (v/v) was used to dehydrate the bacteria. Each dewatering time was 15 min. The bacteria were then embedded and sectioned to a thickness of ~50 nm, and the ultrathin sections were stained with uranyl acetate and lead citrate. The stained sections were mounted on copper grids and observed under a Hitachi HT7700 electron microscope to visualize the spatial dimensions between the assembled bacteria.

Quantitative detection of the bacterial virulence factors

FNA-1 and FNA-2 (500 μl) were added into the different *P. aeruginosa* solution with the OD_{600} value of 0.6 and LB medium of 1.5 ml. Then, the FNA-1–anchored *P. aeruginosa* solution and the FNA-2–anchored *P. aeruginosa* solution were mixed as the experimental groups. The control group consisted of an equal volume of bacterial suspension with noncomplementary FNA pairs and a bacterial suspension containing only 1 ml of tris-HCl buffer with 12.5 mM $MgCl_2$ (20 mM, pH 8.0). After incubating both the experimental and control group samples at 37°C for 24 hours, the supernatant was collected by centrifugation.

To quantitatively detect the rhamnolipids, an equal volume of ether was added to 2 ml of the bacterial supernatant and thoroughly mixed to extract the rhamnolipids. After separating and drying the ether layer, it was redissolved in 200 μl of ultrapure water. Subsequently, 50 μl of this solution was mixed with 450 μl of 0.19% (w/v) 3,5-dihydroxytoluene sulfuric acid solution (1:1, v/v). The mixture was then heated at 80°C for 30 min. After cooling to room temperature, the absorbance of the solution was measured at 421 nm. The concentration of rhamnolipid is proportional to absorbance of the solution at 421 nm (*58*).

According to the protocol of *Pseudomonas* exotoxin A ELISA kit, the exotoxin A was quantitatively detected. Each sample was all tested in triplicate.

Quantitative detection of the inflammatory factors

A549 cells were cultured in Ham's F-12K medium enriched with 10% FBS, penicillin (100 μg/ml), and streptomycin (100 μg/ml) in a 37°C incubator with 5% CO_2. Cultured A549 cells were then seeded at a density of 1×10^4 cells per well in a 96-well plate and incubated at 37°C with 5% CO_2 for 12 hours. After removing the medium, the wells were washed twice with PBS buffer. Subsequently, 100 μl of supernatant from the 24-hour incubated assembled/unassembled bacterial supernatants was added to the A549 cells, respectively, and incubated for an additional 12 hours under the same conditions. Subsequently, the A549 cell supernatants were collected for the detection of inflammatory factors using TNF-α, IL-8, and IL-6 ELISA kits. Each assay was replicated three times per well.

RNA extraction, RNA sequencing, and transcriptomics analysis

Six independent replicates of FNA-treated/untreated culture including *P. aeruginosa*–*P. aeruginosa* and *P. aeruginosa*–*E. coli* were subjected to RNA sequencing analysis. According to the manufacturing's protocols, the total RNA was extracted from the bacterial samples using the TRIzol reagent (Invitrogen, California, USA), following the manufacturer's protocol. RNA integrity and quality were assessed using the Agilent Bioanalyzer 2100 (Agilent, Palo Alto, CA, USA) and NanoDrop spectrophotometer (BIO-DL, Shanghai, China). Libraries were constructed using the NEBNext Ultra RNA Library Prep Kit, and ribosomal RNA (rRNA) was depleted using the Ribo-Zero Plus rRNA Depletion Kit (Illumina, San Diego, CA, USA). Directional libraries were prepared using the NEBNext Ultra Directional RNA Library Prep Kit for Illumina (New England Biolabs, Ipswich, MA, USA) and sequenced on the Illumina NovaSeq 6000 platform (Illumina, San Diego, CA, USA). Cutadapt software was used to remove sequences containing adapters, undetermined bases (marked as N), and low-quality sequences (with a Qphred ≤ 20 accounting for >50% of the read length). To obtain high-quality sequence data (clean reads), sequencing error rates and GC content distribution were checked using FastQC software. Clean reads were mapped to the reference genome of the microbial community using STAR software for genomic localization analysis. The featureCounts tool

of Subread software (version 1.5.0-p3) was used to count the mapped reads. Normalized read counts were obtained using FPKM (fragments per kilobase of transcript per million mapped reads). Differential gene expression analysis was performed using DESeq2 software (version 1.16.1).

Quantitative detection of the QS signal molecules

After culturing the FNA-treated/untreated bacteria at 37°C for 24 hours, the supernatant was collected by centrifugation and filtered using a sterile filter (0.2 μm). To extract QS signal molecules, 1 ml of supernatant was mixed with an equal volume of 1% (v/v) acetic acid–ethanol, vortexed for 30 s, and then centrifuged at 10,000 rpm for 1 min to enhance phase separation. The upper organic phase was collected and then dried at room temperature.

To quantitatively detect C4-HSL and 3-oxo-C12-HSL molecules, an Agilent C18 reverse phase chromatography column (4.6 mm by 250 mm) was used. Initially, different concentrations of standard products were measured using this column to establish a standard curve. Subsequently, the dried samples from both the experimental and control groups were dissolved in 200 μl of chromatographic purity methanol. For chromatographic analysis, a mobile phase consisting of a 50% (v/v) methanol-water solution was used, with a flow rate of 1 ml/min. The detection wavelength was set at 210 nm. For the quantitative detection of PQS molecules, the dried samples from both the experimental and control groups were dissolved in 200 μl of chromatographic purity acetonitrile. Chromatographic analysis was performed using a mobile phase consisting of a 70% (v/v) acetonitrile-water solution, with a flow rate of 1 ml/min. The detection wavelength was also set at 210 nm.

Statistical analyses

All data are presented as means ± SD, and statistical analyses and graphs were performed using OriginLab 9.0 and GraphPad Prism 8.0.1. For comparison of two groups, significance was determined by the two-tailed unpaired Student's *t* test.

Supplementary Materials

This PDF file includes:

Figs. S1 to S25

Tables S1 to S5

REFERENCES AND NOTES

1. K. Faust, J. Raes, Microbial interactions: From networks to models. *Nat. Rev. Microbiol.* **10**, 538–550 (2012).
2. C. Ratzke, J. Barrere, J. Gore, Strength of species interactions determines biodiversity and stability in microbial communities. *Nat. Ecol. Evol.* **4**, 376–383 (2020).
3. M. L. Richard, H. Sokol, The gut mycobiota: Insights into analysis, environmental interactions and role in gastrointestinal diseases. *Nat. Rev. Gastro. Hepat.* **16**, 331–345 (2019).
4. N. Chen, N. Du, W. Wang, T. Liu, Q. Yuan, Y. Yang, Real-time monitoring of dynamic microbial Fe(III) respiration metabolism with a living cell-compatible electron-sensing probe. *Angew. Chem. Int. Ed. Engl.* **61**, e202115572 (2022).
5. G. Chao, T. M. Wannier, C. Gutierrez, N. C. Borders, E. Appleton, A. Chadha, T. Lebar, G. M. Church, helixCAM: A platform for programmable cellular assembly in bacteria and human cells. *Cell* **185**, 3551–3567.e39 (2022).
6. D. S. Glass, I. H. Riedel-Kruse, A synthetic bacterial cell-cell adhesion toolbox for programming multicellular morphologies and patterns. *Cell* **174**, 649–658.e16 (2018).
7. F. J. H. Hol, C. Dekker, Zooming in to see the bigger picture: Microfluidic and nanofabrication tools to study bacteria. *Science* **346**, 1251821 (2014).
8. S. C. Booth, W. P. J. Smith, K. R. Foster, The evolution of short and long-range weapons for bacterial competition. *Nat. Ecol. Evol.* **7**, 2080–2091 (2023).
9. B. Chen, W. Kang, J. Sun, R. Zhu, Y. Yu, A. Xia, M. Yu, M. Wang, J. Han, Y. Chen, L. Teng, Q. Tian, Y. Yu, G. Li, L. You, Z. Liu, Z. Dai, Programmable living assembly of materials by bacterial adhesion. *Nat. Chem. Bio.* **18**, 289–294 (2022).
10. N. Chen, X. Zhang, J. Xi, Y. Yang, Q. Yuan, Recent advances of microbial metabolism analysis: From metabolic molecules to environments. *Sci. China Chem.* **66**, 2941–2950 (2023).
11. L. Niehaus, I. Boland, M. Liu, K. Chen, D. Fu, C. Henckel, K. Chaung, S. E. Miranda, S. Dyckman, M. Crum, S. Dedrick, W. Shou, B. Momeni, Microbial coexistence through chemical-mediated interactions. *Nat. Commun.* **10**, 2052 (2019).
12. D. Song, J. Meng, J. Cheng, Z. Fan, P. Chen, H. Ruan, Z. Tu, N. Kang, N. Li, Y. Xu, X. Wang, F. Shu, L. Mu, T. Li, W. Ren, X. Lin, J. Zhu, X. Fang, M. W. Amrein, W. Wu, L.-T. Yan, J. Lü, T. Xia, Y. Shi, *Pseudomonas aeruginosa* quorum-sensing metabolite induces host immune cell death through cell surface lipid domain dissolution. *Nat. Microbiol.* **4**, 97–111 (2019).
13. N. Chen, D. Cheng, T. He, Q. Yuan, Real-time monitoring of dynamic chemical processes in microbial metabolism with optical sensors. *Chinese J. Chem.* **41**, 1836–1840 (2023).
14. A. J. Stevens, A. R. Harris, J. Gerdts, K. H. Kim, C. Trentesaux, J. T. Ramirez, W. L. McKeithan, F. Fattahi, O. D. Klein, D. A. Fletcher, W. A. Lim, Programming multicellular assembly with synthetic cell adhesion molecules. *Nature* **614**, 144–152 (2023).
15. H. Kim, D. J. Skinner, D. S. Glass, A. E. Hamby, B. A. R. Stuart, J. Dunkel, I. H. Riedel-Kruse, 4-Bit adhesion logic enables universal multicellular interface patterning. *Nature* **608**, 324–329 (2022).
16. Z. Guo, L. Zhang, Q. Yang, R. Peng, X. Yuan, L. Xu, Z. Wang, F. Chen, H. Huang, Q. Liu, W. Tan, Manipulation of multiple cell-cell interactions by tunable DNA scaffold networks. *Angew. Chem. Int. Ed.* **61**, e202111151 (2022).
17. D. S. Glass, U. Alon, Programming cells and tissues. *Science* **361**, 1199–1200 (2018).
18. A. Miano, M. J. Liao, J. Hasty, Inducible cell-to-cell signaling for tunable dynamics in microbial communities. *Nat. Commun.* **11**, 1193 (2020).
19. M. T. Kozlowski, B. R. Silverman, C. P. Johnstone, D. A. Tirrell, Genetically programmable microbial assembly. *ACS Synth. Biol.* **10**, 1351–1359 (2021).
20. A. Doshi, M. Shaw, R. Tonea, S. Moon, R. Minyety, A. Doshi, A. Laine, J. Guo, T. Danino, Engineered bacterial swarm patterns as spatial records of environmental inputs. *Nat. Chem. Biol.* **19**, 878–886 (2023).
21. Y. Wu, C. Fu, C. L. Peacock, S. J. Sorensen, M. A. Redmile-Gordon, K.-Q. Xiao, C. Gao, J. Liu, Q. Huang, Z. Li, P. Song, Y. Zhu, J. Zhou, P. Cai, Cooperative microbial interactions drive spatial segregation in porous environments. *Nat. Commun.* **14**, 4226 (2023).
22. Q. Yi, X. Dai, B. M. Park, J. Gu, J. Luo, R. Wang, C. Yu, S. Kou, J. Huang, R. Lakerveld, F. Sun, Directed assembly of genetically engineered eukaryotic cells into living functional materials via ultrahigh-affinity protein interactions. *Sci. Adv.* **8**, eade0073 (2022).
23. H. Luo, Y. Chen, X. Kuang, X. Wang, F. Yang, Z. Cao, L. Wang, S. Lin, F. Wu, J. Liu, Chemical reaction-mediated covalent localization of bacteria. *Nat. Commun.* **13**, 7808 (2022).
24. H. S. Deter, T. Lu, Engineering microbial consortia with rationally designed cellular interactions. *Curr. Opin. Biotechnol.* **76**, 102730 (2022).
25. M. Xiao, W. Lai, H. Yu, Z. Yu, L. Li, C. Fan, H. Pei, Assembly pathway selection with DNA reaction circuits for programming multiple cell-cell interactions. *J. Am. Chem. Soc.* **143**, 3448–3454 (2021).
26. Y. Du, Y. Lyu, J. Lin, C. Ma, Q. Zhang, Y. Zhang, L. Qiu, W. Tan, Membrane-anchored DNA nanojunctions enable closer antigen-presenting cell-T-cell contact in elevated T-cell receptor triggering. *Nat. Nanotechnol.* **18**, 818–827 (2023).
27. J. Li, K. Xun, K. Pei, X. Liu, X. Peng, Y. Du, L. Qiu, W. Tan, Cell-membrane-anchored DNA nanoplatform for programming cellular interactions. *J. Am. Chem. Soc.* **141**, 18013–18020 (2019).
28. J. Yin, S. Wang, J. Wang, Y. Zhang, C. Fan, J. Chao, Y. Gao, L. Wang, An intelligent DNA nanodevice for precision thrombolysis. *Nat. Mater.* **23**, 854–862 (2024).
29. M. Mao, Z. Lin, L. Chen, Z. Zou, J. Zhang, Q. Dou, J. Wu, J. Chen, M. Wu, L. Niu, C. Fan, Y. Zhang, Modular DNA-origami-based nanoarrays enhance cell binding affinity through the "lock-and-key" interaction. *J. Am. Chem. Soc.* **145**, 5447–5455 (2023).
30. S. Gupta, T. D. Ross, M. M. Gomez, J. L. Grant, P. A. Romero, O. S. Venturelli, Investigating the dynamics of microbial consortia in spatially structured environments. *Nat. Commun.* **11**, 2418 (2020).
31. J. van Gestel, T. Bareia, B. Tenennbaum, A. D. Co, P. Guler, N. Aframian, S. Puyesky, I. Grinberg, G. G. D'Souza, Z. Erez, M. Ackermann, A. Eldar, Short-range quorum sensing controls horizontal gene transfer at micron scale in bacterial communities. *Nat. Commun.* **12**, 2324 (2021).
32. Y. Jiang, R. Wu, W. Zhang, F. Xin, M. Jiang, Construction of stable microbial consortia for effective biochemical synthesis. *Trends Biotechnol.* **41**, 1430–1441 (2023).
33. S. E. Darch, O. Simoska, M. Fitzpatrick, J. P. Barraza, K. J. Stevenson, R. T. Bonnecaze, J. B. Shear, M. Whiteley, Spatial determinants of quorum signaling in a *Pseudomonas aeruginosa* infection model. *P. Natl. Acad. Sci. U.S.A.* **115**, 4779–4784 (2018).
34. L. Wang, X. Wang, Y. Wu, M. Guo, C. Gu, C. Dai, D. Kong, Y. Wang, C. Zhang, D. Qu, C. Fan, Y. Xie, Z. Zhu, Y. Liu, D. Wei, Rapid and ultrasensitive electromechanical detection of ions, biomolecules and SARS-CoV-2 RNA in unamplified samples. *Nat. Biomed. Eng.* **6**, 276–285 (2022).

35. X. Shi, J. Zhang, F. He, A new aptamer/polyadenylated DNA interdigitated gold electrode piezoelectric sensor for rapid detection of *Pseudomonas aeruginosa*. *Biosens Bioelectron.* **132**, 224–229 (2019).
36. D. Lu, G. Zhu, X. Li, J. Xiong, D. Wang, Y. Shi, T. Pan, B. Li, L. P. Lee, H. Xin, Dynamic monitoring of oscillatory enzyme activity of individual live bacteria via nanoplasmonic optical antennas. *Nat. Photonics* **17**, 904–911 (2023).
37. N. Chen, N. Du, R. Shen, T. He, J. Xi, J. Tan, G. Bian, Y. Yang, T. Liu, W. Tan, L. Yu, Q. Yuan, Redox signaling-driven modulation of microbial biosynthesis and biocatalysis. *Nat. Commun.* **14**, 6800 (2023).
38. S. Moreno-Gamez, M. E. Hochberg, G. S. van Doorn, Quorum sensing as a mechanism to harness the wisdom of the crowds. *Nat. Commun.* **14**, 3415 (2023).
39. P. Moura-Alves, A. Puyskens, A. Stinn, M. Klemm, U. Guhlich-Bornhof, A. Dorhoi, J. Furkert, A. Kreuchwig, J. Protze, L. Lozza, G. Pei, P. Saikali, C. Perdomo, H. J. Mollenkopf, R. Hurwitz, F. Kirschhoefer, G. Brenner-Weiss, J. Weiner III, H. Oschkinat, M. Kolbe, G. Krause, S. H. E. Kaufmann, Host monitoring of quorum sensing during *Pseudomonas aeruginosa* infection. *Science* **366**, eaaw1629 (2019).
40. J. K. Kim, Y. Chen, A. J. Hirning, R. N. Alnahhas, K. Josić, M. R. Bennett, Long-range temporal coordination of gene expression in synthetic microbial consortia. *Nat. Chem. Biol.* **15**, 1102–1109 (2019).
41. V. C. Ozgen, W. Kong, A. E. Blanchard, F. Liu, T. Lu, Spatial interference scale as a determinant of microbial range expansion. *Sci. Adv.* **4**, eaau0695 (2018).
42. K. Zhao, W. Li, J. Li, T. Ma, K. Wang, Y. Yuan, J. S. Li, R. Xie, T. Huang, Y. Zhang, Y. Zhou, N. Huang, W. Wu, Z. Wang, J. Zhang, B. Yue, Z. Zhou, J. Li, Y.-Q. Wei, X. Zhang, X. Zhou, TesG is a type I secretion effector of *Pseudomonas aeruginosa* that suppresses the host immune response during chronic infection. *Nat. Microbiol.* **4**, 459–469 (2019).
43. C. J. Harding, M. Bischoff, M. Bergkessel, C. M. Czekster, An anti-biofilm cyclic peptide targets a secreted aminopeptidase from *P. aeruginosa*. *Nat. Chem. Biol.* **19**, 1158–1166 (2023).
44. D. R. Plichta, D. B. Graham, S. Subramanian, R. J. Xavier, Therapeutic opportunities in inflammatory bowel disease: Mechanistic dissection of host-microbiome relationships. *Cell* **178**, 1041–1056 (2019).
45. P. Gao, K. Guo, Q. Pu, Z. Wang, P. Lin, S. Qin, N. Khan, J. Hur, H. Liang, M. Wu, oprC impairs host defense by increasing the quorum-sensing-mediated virulence of *Pseudomonas aeruginosa*. *Front. Immunol.* **11**, 1696 (2020).
46. S. Qin, W. Xiao, C. Zhou, Q. Pu, X. Deng, L. Lan, H. Liang, X. Song, M. Wu, *Pseudomonas aeruginosa*: Pathogenesis, virulence factors, antibiotic resistance, interaction with host, technology advances and emerging therapeutics. *Signal Transduct. Target Ther.* **7**, 199 (2022).
47. M.-K. Lee, Y. Lee, J.-W. Huh, H. Chen, W. Wu, U.-H. Ha, The *Pseudomonas aeruginosa* HSP90-like protein HtpG regulates IL-8 expression through NF-κB/p38 MAPK and CYLD signaling triggered by TLR4 and CD91. *Microbes Infect.* **22**, 558–566 (2020).
48. D. Ruano-Gallego, J. Sanchez-Garrido, Z. Kozik, E. Núñez-Berrueco, M. Cepeda-Molero, C. Mullineaux-Sanders, Y. N. Baghshomali, S. L. Slater, N. Wagner, I. Glegola-Madejska, T. I. Roumeliotis, T. Pupko, L. Á. Fernández, A. Rodríguez-Patón, J. S. Choudhary, G. Frankel, Type III secretion system effectors form robust and flexible intracellular virulence networks. *Science.* **371**, eabc9531 (2021).
49. S. K. Chuang, G. D. Vrla, K. S. Fröhlich, Z. Gitai, Surface association sensitizes *Pseudomonas aeruginos*a to quorum sensing. *Nat. Commun.* **10**, 4118 (2019).
50. M. Whiteley, S. P. Diggle, E. P. Greenberg, Progress in and promise of bacterial quorum sensing research. *Nature* **551**, 313–320 (2017).
51. V. Chubukov, L. Gerosa, K. Kochanowski, U. Sauer, Coordination of microbial metabolism. *Nat. Rev. Microbiol.* **12**, 327–340 (2014).
52. V. R. Marcelino, C. Welsh, C. Diener, E. L. Gulliver, E. L. Rutten, R. B. Young, E. M. Giles, S. M. Gibbons, C. Greening, S. C. Forster, Disease-specific loss of microbial cross-feeding interactions in the human gut. *Nat. Commun.* **14**, 6546 (2023).
53. L. Ona, S. Giri, N. Avermann, M. Kreienbaum, K. M. Thormann, C. Kost, Obligate cross-feeding expands the metabolic niche of bacteria. *Nat. Ecol. Evol.* **5**, 1224–1232 (2021).
54. T. Christofi, S. Panayidou, I. Dieronitou, C. Michael, Y. Apidianakis, Metabolic output defines *Escherichia coli* as a health-promoting microbe against intestinal *Pseudomonas aeruginosa*. *Sci. Rep.* **9**, 14463 (2019).
55. A. Gatsios, C. S. Kim, J. M. Crawford, *Escherichia coli* small molecule metabolism at the host-microorganism interface. *Nat. Chem. Biol.* **17**, 1016–1026 (2021).
56. K. B. Said, A. Alsolami, A. M. Khalifa, N. A. Khalil, S. Moursi, A. Osman, D. Fahad, E. Rakha, M. Rashidi, S. Moussa, A. I. Bashir, F. Alfouzan, S. Hammam, T. E. Taha, A. Al-hazimi, A. Al Jadani, Ha'il COM Research Unit Group, A multi-point surveillance for antimicrobial resistance profiles among clinical isolates of Gram-negative bacteria recovered from major Ha'il hospitals, Saudi Arabia. *Microorganisms* **9**, 2024 (2021).
57. Y. Yang, B. Zeng, J. Guo, Y. Li, Y. Yang, Q. Yuan, Two-dimensional device with light-controlled capability for treatment of cancer-relevant infection diseases. *Anal. Chem.* **92**, 10162–10168 (2020).
58. C. W. Thio, W. H. Lim, U. K. Md. Shah, L. Y. Phang, Palm kernel fatty acid distillate as substrate for rhamnolipids production using *Pseudomonas* sp. LM19. *Green Chem. Lett. Rev.* **15**, 83–92 (2022).

Acknowledgments: We thank the Core Facility of Wuhan University for SEM and TEM analysis. **Funding:** This work was supported by the National Natural Science Foundation of China (21925401 to Q.Y., 52221001 to Q.Y., and 22322408 to Y.Y.); National Key R&D Program of China (2023YFF1205900 to Q.Y. and 2021YFA1202400 to Y.Y); Hunan Provincial Key Research and Development Plan (2024JK2117 to Q.Y.); "Sharp Knife" Technology Research Program of Hubei Province (2023BAA002 to Q.Y); Fundamental Research Funds for the Central Universities (2042022rc0004 to Q.Y.); China Postdoctoral Science Foundation (2024M752456 to N.C.); Postdoctoral Innovative Research of Hubei Province of China (211000025 to N.C.); New Cornerstone Science Foundation through the XPLORER PRIZE; and Interdisciplinary Innovative Talents Foundation from Renmin Hospital of Wuhan University. **Author contributions:** Conceptualization: N.C., Q.Y., W.T., L.Y., and Y.Z. Methodology: N.C., J.X, N.D., R.S., and R.Z. Investigation: N.C., N.D., and J.X. Visualization: N.D. and R.S. Supervision: Q.Y., W.T., and L.Y. Writing—original draft: N.C., J.X., N.D., and W.H. Writing—review and editing: N.C., Q.Y., Y.Y., Y.Z., L.Y., and T.P. **Competing interests:** The authors declare that they have no competing interests. **Data and materials availability:** All data needed to evaluate the conclusions in the paper are present in the paper and/or the Supplementary Materials.

Submitted 2 July 2024
Accepted 7 November 2024
Published 11 December 2024
10.1126/sciadv.adr4399